THEODORSEN'S METHOD:
A NUMERICAL CONFORMAL MAP APPLIED TO FLUID DYNAMICS

A Thesis by

Mathew Tucker

Bachelor of Mathematics, University of North Georgia, December 2017

Submitted to the Department of Mathematics, Statistics, and Physics
and the faculty of the Graduate School of
Wichita State University
in partial fulfillment of
the requirements for the degree of
Master of Science

May 2023

THEODORSEN'S METHOD:
A NUMERICAL CONFORMAL MAP APPLIED TO FLUID DYNAMICS

The following faculty members have examined the final copy of this thesis for form and content, and recommend that it be accepted in partial fulfillment of the requirement for the degree of Master of Science with a major in Mathematics.

Thomas K. DeLillo, Committee Chair

Christopher C. Green, Committee Member

Leonard S. Miller, Committee Member

ABSTRACT

The details of Theodorsen's method for computing the conformal map from the exterior of the unit disk to the exterior of a simple closed curve in the complex plane are reviewed. An implementation of the method in Matlab is presented and used to compute potential flow over a single airfoil. Pressure curves and circulations for flows satisfying the Kutta condition at the trailing edge of the airfoil are calculated and the results are compared to output from a standard engineering code.

ACKNOWLEDGEMENTS

The author would like to say thank you to Vijay Matheswaran for generously providing data from [12].

TABLE OF CONTENTS

Chapter **Page**

TABLE OF CONTENTS (continued)

Chapter **Page**

LIST OF FIGURES

Figure **Page**

LIST OF FIGURES (continued)

Figure **Page**

CHAPTER 1

Introduction

1.1 Introduction

The purpose of this thesis is to present the details of Theodorsen's method [14, 11] for computing the conformal map from the exterior of the unit disk to the exterior of a simple closed curve in the complex plane. An implementation of the method and supporting functions in MATLAB are presented and explained below. The basics of the complex velocity potential and its computation are also reviewed and used to compute potential-flow over a single airfoil. The pressure curve and circulation for flows satisfying the Kutta condition at the trailing edge of the airfoil are calculated, and the results are compared to output from a standard engineering code [12]. Most of the background material presented here is available, for example, in [2, 4, 5, 11]. However, we collect it here for completeness.

Conformal maps have frequently been used in the past for airfoil analysis [10]. Recently, newer methods for computing conformal maps and solving potential theory problems in multiply connected domains have been developed and applied to airfoil calculations [7, 8]. This thesis considers only the simply connected case, and the calculations here, and in planned future work using similar methods [6], are meant to provide guidance and benchmark studies for the ongoing efforts by DeLillo and his co-workers to compute flow over multielement airfoils. Even though modern CFD codes are available, these classical conformal mapping methods can provide a useful tool for early stages of the design process.

1.2 Outline

The main task is to use MATLAB code to apply Theodorsen's method to compute potential flows over a single airfoil by conformally mapping streamlines in the circle domain to streamlines in the airfoil domain. You can refer to chapters 1 through 5 for all of the

necessary background material in complex analysis, Fourier series, conformal mapping, and potential flow.

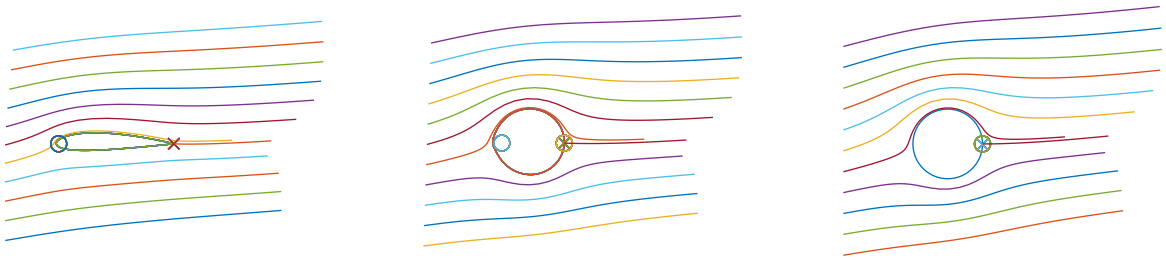

Figure 1.2.1: The following are graphs of the potential flow, assuming a 7° angle of attack, about the NACA 2415 airfoil (left), the image of the airfoil under Karman-Trefftz (center), and the unit circle.

Here is a brief outline of the thesis:

In chapter 2, we will motivate our work by reviewing the fluid dynamic concepts used in this paper, such as potential flow, circulation, and the Kutta condition.

In chapters 3, 4 and 5, we review material related to conformal maps, numerical methods, and Theodorsen's method. Our reason for doing this is because, in order to map to the exterior of an airfoil, the explicit Karman-Trefftz transformation k must first be applied to smooth the corner at the trailing edge of the airfoil. This map will produce a number of points on a curve γ which is more nearly circular where Theodorsen's method can be applied. The boundary of the domain produced by the Karman-Trefftz map must then be parametrized by the argument ϕ of the boundary point with respect to an interior point (say at 0). This will be done with a periodic cubic spline fit. Then Theordorsen's method will produce a conformal map $w = h(z)$ mapping the exterior of the unit disk to the exterior of the curve γ. The map f from the exterior of the unit disk to the exterior of the airfoil is then

$$f(z) = k^{-1}(h(z)),$$

where k^{-1} is the inverse of the Karman-Trefftz map, which is given by an explicit analytic formula.

In chapter 6, we want to use the output of the codes implemented above to calculate quantities of interest to designers of airfoils, such as pressure curves and streamlines.

CHAPTER 2

Fluid Dynamics

2.1 Introduction

The following chapter is a brief overview of discussions in [2, 4]. Since we will be making use of conformal maps (see Chapter 3), we will refer to the circle domain as the z-plane and the physical domain as the Z-plane.

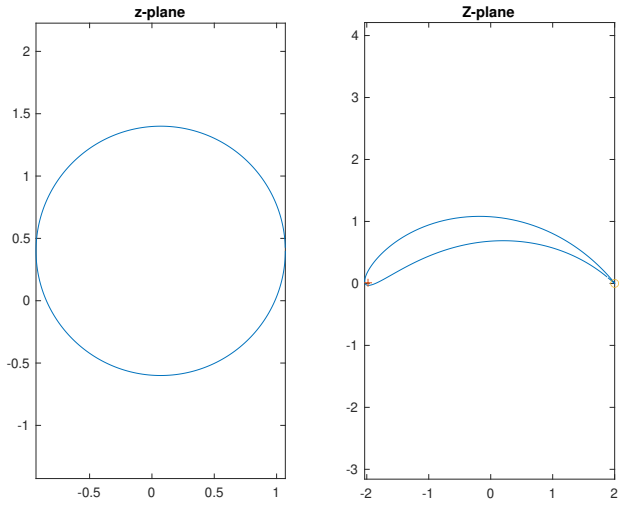

Figure 2.1.1: The graph on the left is of the image of an airfoil in the circle domain and the graph on the right is of the airfoil in the physical domain.

2.2 Plotting Streamlines

A streamline, at fixed time t, is a curve which lies tangent to the instantaneous velocity $\mathbf{u}(\mathbf{x}, t)$ at each point $\mathbf{x}$. Hence, for fixed time t, a streamline $x = x(s),\ y = y(s)$ is the solution to

$$\frac{dx}{u} = \frac{dy}{v} = ds.$$

However, since in the case of steady flow streamlines coincide with the particle path of the fluid, we can write

$$\frac{dx}{u} = \frac{dy}{v} = dt.$$

For that reason, as $w'(z) = u - iv$ (see in Sec 2.3), we obtained the streamlines by solving the system

$$\begin{aligned} \frac{dx}{dt} &= u = \mathrm{Re}\{w'(z)\} \\ \frac{dy}{dt} &= v = -\mathrm{Im}\{w'(z)\} \end{aligned}$$

numerically using the MATLAB solver `ode45`. This allows us to display streamlines originating near the stagnation points at the trailing edges. The streamlines in the circle domain, where $\mathrm{Im}\{w(z)\}$ is constant, are then conformally mapped by $Z = f(z)$ to streamlines on their physical domain

$$\mathrm{Im}\{W(Z)\} = \mathrm{Im}\{W\left(f(z)\right)\} = \mathrm{Im}\{w(z)\}.$$

2.3 Complex Velocity Potential

Given that our flow must be incompressible we have

$$u = \partial_y \psi \quad v = -\partial_x \psi$$

and from irrotationality we have that

$$\mathbf{u} = \nabla \phi.$$

Together these conditions lead us to conclude the velocity field can be represented by equations

$$u = \partial_x \phi = \partial_y \psi, \quad v = \partial_y \phi = -\partial_x \psi.$$

But these are exactly the Cauchy-Riemann equations for the complex potential,

$$w(z) = \phi(x, y) + i\psi(x, y),$$

where the function $w(z)$ is analytic in $z = x + iy$, ϕ is the potential, and ψ is the stream function. Moreover, since $(u, v) = (\phi_x, \phi_y) = (\psi_y, -\psi_x)$ we find that the conjugate complex velocity is,

$$\frac{dw}{dz} = \phi_x + i\psi_x = \phi_x - i\phi_y = u(x, y) - iv(x, y)$$

with flow speed, $\left|\frac{dw}{dz}\right|$ given by

$$\left|\frac{dw}{dz}\right|^2 = \frac{dw}{dz}\overline{\frac{dw}{dz}} = u^2 + v^2.$$

Let us now establish, for the purposes of demonstrating key concepts from this chapter, the example of potential flow past a circular cylinder of radius a centered on the origin with an angle of attack $\alpha = 0$ and superimpose circulation of arbitrary strength Γ

$$w(z) = U\left(z + \frac{a^2}{z}\right) - i\frac{\Gamma \log(z)}{2\pi},$$

where U is the flow speed. Rewriting $w(z)$ as

$$w(z) = U\left(x + iy + \frac{a^2}{x + iy}\right) - i\frac{\Gamma \log(x + iy)}{2\pi}$$

we immediately find the we can rewrite the complex flow potential in the form $w(z) = \phi(x, y) + i\psi(x, y)$ to get,

$$w(z) = \left[U\left(x + \frac{xa^2}{x^2 + y^2}\right) + \frac{\Gamma}{2\pi}\arg(x + iy)\right] - i\left[U\left(y - \frac{ya^2}{x^2 + y^2}\right) + \frac{\Gamma}{4\pi}\log\left(x^2 + y^2\right)\right].$$

Then by application of the Cauchy-Riemann equations we get,

$$\begin{cases} \phi_x(x, y) = \frac{a^2U\left(y^2 - x^2\right)}{(x^2+y^2)^2} + \frac{2\pi U(x^2+y^2)+\Gamma y}{2\pi(x^2+y^2)} \\ \psi_y(x, y) = \frac{a^2U\left(y^2 - x^2\right)}{(x^2+y^2)^2} + \frac{2\pi U(x^2+y^2)+\Gamma y}{2\pi(x^2+y^2)} \end{cases}$$

and

$$\begin{cases} \phi_y(x, y) = \frac{2a^2Uxy}{(x^2+y^2)^2} + \frac{\Gamma x}{2\pi(x^2+y^2)} \\ -\psi_x(x, y) = \frac{2a^2Uxy}{(x^2+y^2)^2} + \frac{\Gamma x}{2\pi(x^2+y^2)} \end{cases}.$$

Hence $\phi_x(x, y) = \psi_y(x, y)$ and $\phi_y(x, y) = -\psi_x(x, y)$ and $w(z)$ is analytic.

2.4 Bernoulli's Equation

Bernoulli's equation is a result in fluid dynamics which provides a relation between changes in pressure, density, and velocity of a fluid.

Theorem 2.4.1. *As the velocity of a fluid* $\left|\frac{dw}{dz}\right|$ *increases the pressure* P *within the fluid decreases according to the following relation,*

$$P + \frac{\rho |dw/dz|^2}{2} = C$$

Applying this to our example, we find that since

$$w'(z) = U\left(1 - \frac{a^2}{z^2}\right) - \frac{i\Gamma}{2\pi z}$$

we get the following relation

$$P + \frac{\rho \left|U\left(1 - \frac{a^2}{z^2}\right) - \frac{i\Gamma}{2\pi z}\right|^2}{2} = C$$

2.5 Circulation

The circulation Γ around a simple closed curve about the origin is defined as,

$$\Gamma = \int_C \mathbf{u} \cdot d\mathbf{x}.$$

Applying this to our example,

$$\int_C \mathbf{u} \cdot d\mathbf{x} = \int_C \mathrm{Re}\left[udx + vdy + i\left(udy - vdx\right)\right] = \mathrm{Re}\int_C (u - iv)dz = \mathrm{Re}\int_C w'(z)dz =$$

$$\mathrm{Re}\int_C \left[U\left(1 - \frac{a^2}{z^2}\right) - \frac{i\Gamma}{2\pi z}\right] dz.$$

But by residue theorem we know $\int_C U\left(1 - \frac{a^2}{z^2}\right) dz = 0$, and so we have that

$$\mathrm{Re}\int_C \left[U\left(1 - \frac{a^2}{z^2}\right) - \frac{i\Gamma}{2\pi z}\right] dz = -\mathrm{Re}\left[\frac{i\Gamma}{2\pi} i2\pi\right] = \Gamma.$$

Hence Γ is the circulation of $w(z)$ about C.

2.6 Kutta Condition

The Kutta condition is the requirement that at the trailing edge of an airfoil, the flow must separate smoothly, without any abrupt changes in direction or pressure. Mathematically this is equivalent to taking the circulation at the trailing edge of an airfoil to be finite.

Now, before we move on to an example, it will be convenient for us to use a different example then the one previously established. Let us consider uniform flow past a flat plate of length 4 with an angle of attack α. Observe that the map from the circle domain (z-plane) to the physical domain (Z-plane) is

$$Z = z + \frac{1}{z} = f(z).$$

Then, in the circle domain the complex potential is

$$w(z) = U\left(ze^{-i\alpha} + \frac{1}{z}e^{i\alpha}\right) - i\frac{\Gamma \log(z)}{2\pi}.$$

It follows then, as $W(Z) = w(f^{-1}(Z))$, that $\frac{dW}{dZ} = \frac{dw}{dz}/\frac{dZ}{dz}$. Differentiating we find

$$\begin{cases} \frac{dw}{dz} = U\left(e^{-i\alpha} - \frac{1}{z^2}e^{i\alpha}\right) - i\frac{\Gamma}{2\pi z} \\ \frac{dZ}{dz} = 1 - \frac{1}{z^2}, \end{cases}$$

hence we get that

$$\frac{dW}{dZ} = \left(Ue^{-i\alpha} - \frac{U}{z^2}e^{i\alpha} - i\frac{\Gamma}{2\pi z}\right) / \left(1 - \frac{1}{z^2}\right).$$

But notice, $\frac{dW}{dZ} \to \infty$ at the ends of our plate ($Z = \pm 2$, $z = \pm 1$). The Kutta-Condition selects the physical Γ as the one which eliminates these singularities by setting

$$Ue^{-i\alpha} - Ue^{i\alpha} - i\frac{\Gamma}{2\pi} = 0$$

or

$$\Gamma = -4\pi U \sin(\alpha).$$

CHAPTER 3

Conformal Maps

3.1 Conformal Maps to Exterior Domains

Theorem 3.1.1. *If $f(z)$ is analytic in $|z| > 1$, continuous for $|z| \geq 1$, and $h(\infty) = 0$, then for $|z| > 1$*

$$f(z) = -\frac{1}{2\pi i}\int_{|\zeta|=1} \frac{f(\zeta)}{\zeta - z} d\zeta,$$

where the unit circle $|\zeta| = 1$ is traversed in the counterclockwise direction.

Proof 3.1.1. Given a conformal map f that is analytic in $|z|$, continuous for $|z| \geq 1$, and $f(\infty) = 0$, then by the previous theorem for $|z| > 0$ we have that,

$$f(z) = \frac{-1}{2\pi i}\int_{|\zeta|=1} \frac{f(\zeta)}{\zeta - z} d\zeta. \tag{3.1}$$

Observe, by a simple rearrangement we can write,

$$f(z) = \frac{1}{2\pi i}\int_{|\zeta|=1} \frac{f(\zeta)}{1 - \zeta/z} \frac{d\zeta}{z}.$$

So, since $\sum_{n=0} \xi^n = \frac{1}{1-\xi}$ for $|\xi| < 1$ and $|\zeta/z| < 1$, it follows that we can write (3.1) in the form,

$$f(z) = \frac{1}{2\pi i}\int_{|\zeta|=1} f(\zeta) \sum_{n=1} (\zeta/z)^n \frac{d\zeta}{\zeta}.$$

But, $d\zeta = ie^{i\varphi} d\varphi$ and $|\zeta| = 1$, so we get

$$f(z) = \frac{1}{2\pi}\int_0^{2\pi} h(ie^{i\varphi}) \sum_{n=1} \frac{e^{in\varphi}}{z^n} d\varphi.$$

$$= \sum_{n=1} z^{-n} \frac{1}{2\pi}\int_0^{2\pi} f(ie^{i\varphi}) e^{-i(-n)\varphi} d\varphi.$$

So (3.1) is exactly equal to

$$f(z) = \sum_{n=1} \hat{f}_{-n} z^{-n},$$

where $\hat{f}_n$ are the Fourier coefficients of $h(e^{i\varphi})$. ■

3.2 Karman-Trefftz Transformation

Unfortunately since airfoils are slender and contain a corner at their trailing edge, we can not apply Theodoren's Method directly to an airfoil as it requires that our curve be nearly circular. Instead, we apply a Karman-Trefftz transformation which smooths the corner at the trailing edge and maps the exterior of our airfoil to the exterior of a nearly circular curve. The Karman-Trefftz transformation

$$\frac{\zeta - \zeta_1}{\zeta - \zeta_2} = \left(\frac{z - z_1}{z - z_2}\right)^{1/\beta},$$

where z_1 is the location of a corner with exterior angle $\beta\pi$ on some closed curve and z_2 is a point to the interior of the closed curve, maps z_1 to ζ_1 and z_2 to ζ_2. Moreover, provided that z_2 is chosen to be a point sufficiently close to the leading edge, the map

$$k(z) = \frac{\zeta_1 - \zeta_2 \left(\frac{z-z_1}{z-z_2}\right)^{1/\beta}}{1 - \left(\frac{z-z_1}{z-z_2}\right)^{1/\beta}} = \zeta$$

results in a nearly circular closed curve.

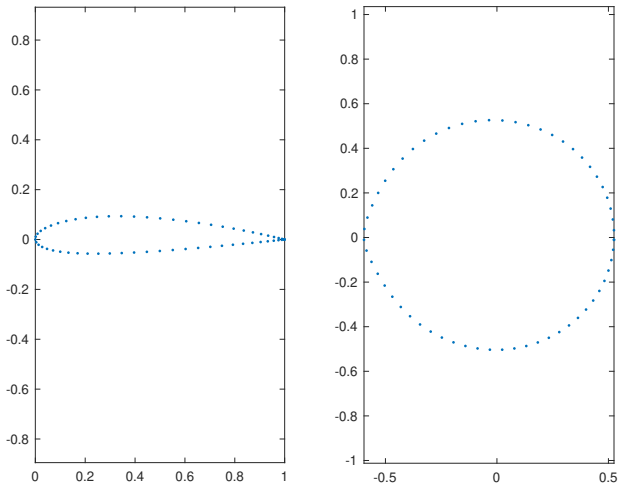

Figure 3.2.1: Points along the boundary of a NACA 2415 airfoil before and after the application of the Karman-Trefftz map and centered at the origin.

Due to the importance of the derivatives at infinity of conformal maps (to and from the physical and circle domains) in determining the strength and orientation of the singularities of the complex potential, we will now turn our attention now to the derivative of $k(z)$ at ∞. For brevity, let us write

$$\kappa(z) = \left(\frac{z - z_1}{z - z_2}\right)^{1/\beta}$$

then

$$k(z) = \frac{\zeta_1 - \zeta_2\kappa(z)}{1 - \kappa(z)}.$$

But as $\kappa(z) = \left(\frac{1-z_1/z}{1-z_2/z}\right)^{1/\beta}$ and $(1-x)^\alpha = 1 - \alpha x + \mathcal{O}(x^2)$ for $|x| < 1$ we can write

$$\kappa(z) = \frac{1 - z_1(\beta z)^{-1} + \mathcal{O}(z^{-2})}{1 - z_2(\beta z)^{-1} + \mathcal{O}(z^{-2})}.$$

So, for $z \to \infty$ we find

$$\kappa(z) \to 1 - \frac{z_1 - z_2}{\beta z} + \mathcal{O}(z^{-2})$$

and

$$k(z) \to \frac{\beta(\zeta_1 - \zeta_2)}{z_1 - z_2} z.$$

Thus we get that

$$k'(\infty) = \frac{\beta(\zeta_1 - \zeta_2)}{z_1 - z_2} = \frac{1}{(k^{-1})'(\infty)}.$$

Since we are interested in conformally mapping data from the physical domain to the circle domain and conformally mapping solutions in the circle domain back to the physical domain, we will also require the use of the inverse Karman-Trefftz map

$$k^{-1}(\zeta) = \frac{z_1 - z_2\left(\frac{\zeta-\zeta_1}{\zeta-\zeta_2}\right)^\beta}{1 - \left(\frac{\zeta-\zeta_1}{\zeta-\zeta_2}\right)^\beta} = z$$

with derivative at infinity,

$$(k^{-1})'(\infty) = \frac{1}{\beta}\frac{z_2 - z_1}{\zeta_2 - \zeta_1} = \frac{1}{k'(\infty)}.$$

The complex velocity potential $W(Z)$ in the physical (airfoil) Z-plane in terms of the velocity potential $w(z)$ in the circle domain and the conformal map $Z = f(z)$ is

$$W(Z) = W(f(z)) = w(z) = w(f^{-1}(Z)).$$

Therefore, $\frac{dw}{dz}$ is given by

$$\overline{\frac{dw}{dz}} = \frac{dW}{dZ} = \frac{d}{dZ} w(f^{-1}(Z)) = w'(z)\frac{dz}{dZ} = w'(z)/f'(z).$$

For uniform velocity U_Z at ∞ in the physical Z-plane, we need

$$\overline{U}_Z = w'(\infty)/f'(\infty) = \overline{U}/f'(\infty),$$

where U is the uniform velocity in the circle z-plane. Note that, since $f(z) = k^{-1}(h(z))$,

$$f'(z) = (k^{-1})'(h(z))h'(z).$$

The auxiliary function for exterior of the unit disk

$$h(z) = \sum_{k=-1}^{\infty} a_{-k} z^{-k} = a_1 z + a_0 + O(1/z)$$

has $h'(\infty) = a_1$. For a single inverse Karman-Trefftz map, $k^{-1}(\zeta)$, a calculation gives

$$(k^{-1})'(\infty) = \frac{1}{\beta}\left(\frac{z_2 - z_1}{\zeta_2 - \zeta_1}\right).$$

Therefore, we need

$$\overline{U} = \overline{U}_Z f'(\infty) = \overline{U}_Z \left(\frac{z_2 - z_1}{\zeta_2 - \zeta_1}\right) a_1/\beta.$$

This is currently implemented in the Matlab function `velocityd.m` where the right hand side for `ode45` is computed and the derivative at infinity is passed as a global variable `derinf`.

3.2.1 Code

For Karman-Trefftz there are two functions we need to form:

1. KarmanTrefftz - the forward map;

2. invKT - the inverse map.

Karman-Trefftz:

```
function zeta = KarmanTrefftz(z,z1,z2,zeta1,zeta2,delta)
    %Karman-Trefftz from z to zeta plane
     w = ((z(1)-z1)/(z(1)-z2))^delta;
     zeta(1) = (zeta1 - zeta2*w)./(1-w);
     w = ((z(2)-z1)/(z(2)-z2))^delta;
     zeta(2) = (zeta1 - zeta2*w)./(1-w);
    for j=3:length(z)
        branch = w;
        w = ((z(j)-z1)/(z(j)-z2));
        w = crootbr(w,branch,delta);
        zeta(j) = (zeta1 - zeta2*w)/(1-w);
    end
end
```

Inverse Karman-Trefftz:

```
function z = invKT(zeta,z1,z2,zeta1,zeta2,delta)
    % Karman-Trefftz from z to zeta plane
    w = ((zeta-zeta1)./(zeta-zeta2)).^(1/delta);
    z = (z1 - z2.*w)./(1-w);
end
```

crootbr:

```
function zb = crootbr(z,branch,delta)
% choosing continuous complex branch of delta root
b1=real(branch);
b2=imag(branch);
z=z^delta;
q=real(z);
r=imag(z);
if (q*b1+r*b2<0)
    zb=z*exp(-i*2*pi*delta);
else
    zb=z;
end
end
```

velocityd:

```
function ydot = velocityd(t,y)
% velocity from complex potential
global derinf
z = y(1)+1i*y(2);
U = 1;
degrees = 10
alpha = degrees*pi/180;
cvel = U*exp(-1i*alpha); % rotate velocity at infinity
cvel = cvel*derinf;
circ = -2*imag(cvel); % circulation to make z=1 at stagnation point (trailing
    edge)
dwdz = cvel - conj(cvel)./z.^2 + circ*1i./z;  % stream plus circulation
ydot = [real(dwdz);-imag(dwdz)];
end
```

CHAPTER 4

Numerical Analysis

4.1 Discrete Fourier Transform (DFT) and Fast Fourier Transform (FFT)

Recall, the coefficients of the Fourier series for the periodic function $f(x)$ are found via the form,

$$c_k \coloneqq \frac{1}{2\pi}\int_0^{2\pi} f(x)e^{-ixk}dx.$$

Approximating these coefficient via the trapezoidal rule we find

$$c_k \approx \frac{1}{2\pi}\left(\frac{1}{2}f(x_0) + \sum_{j=1}^{n-1} f(x_j)e^{-ikj\frac{2\pi}{n}} + \frac{1}{2}f(x_n)e^{-ik2\pi}\right)\frac{2\pi}{n} = \frac{1}{n}\sum_{j=0}^{n-1} f(x_j)e^{-ikj\frac{2\pi}{n}} = \hat{c}_k.$$

It is worth noting, since

$$w_n^{-j(k-n)} = w_n^{-jk}w_n^{jn} = w_N^{-jk}$$

we get that $\hat{c}_k = \hat{c}_{k-n}$. Thus the discrete Fourier coefficients are n-periodic, $\hat{c}_k = \hat{c}_{k\pm n}$. Moreover, observe if we set

$$F_n = \left[w_n^{-jk}\right]_{j,k=0,\cdots,n-1} = \begin{bmatrix} 1 & 1 & 1 & \cdots & 1 \\ 1 & w_n^{-1} & w_n^{-2} & \cdots & w_n^{-n+1} \\ 1 & w_n^{-2} & w_n^{-4} & \cdots & w_n^{-2(n-1)} \\ \vdots & \vdots & \vdots & \ddots & \vdots \\ 1 & w_n^{-n+1} & w_n^{-2(n-1)} & \cdots & w_n^{-(n-1)^2} \end{bmatrix}, \hat{\mathbf{c}} = \begin{bmatrix} \hat{c}_0 \\ \hat{c}_1 \\ \vdots \\ \hat{c}_{n-1} \end{bmatrix}, \hat{\mathbf{f}} = \begin{bmatrix} f_0 \\ f_1 \\ \vdots \\ f_{n-1} \end{bmatrix},$$

with $f_k = f(x_k)$, then we can write $\hat{\mathbf{c}} = \frac{1}{n}F_n\hat{\mathbf{f}}$ the matrix form of the discrete Fourier transform.

Observe, as our series has a finite number of terms we can increase the computational speed of our algorithm by making use of the fact that we can break our series up into odd and even terms. So that, for $N = \frac{n}{2}$,

$$\hat{c}_k = \frac{1}{n}\sum_{j=0}^{n-1} f_j w_n^{-jk}$$

$$= \frac{1}{n}\sum_{j=0}^{N-1} f_{2j} w_n^{-2jk} + \frac{1}{n}\sum_{j=0}^{N-1} f_{2j+1} w_n^{-(2j+1)k}$$

$$= \frac{1}{n}\sum_{j=0}^{N-1} f_{2j} w_n^{-2jk} + \frac{w_n^{-k}}{n}\sum_{j=0}^{N-1} f_{2j+1} w_n^{-2jk}.$$

By the n-periodicity of $\hat{c}_k = \hat{c}_{k-n}$, we have the canonical form of the fast Fourier transform,

$$\hat{c}_k = \frac{1}{n}\sum_{j=0}^{N-1} f_{2j} w_{\frac{n}{2}}^{-jk} + \frac{w_n^{-k}}{n}\sum_{j=0}^{N-1} f_{2j+1} w_{\frac{n}{2}}^{-jk}.$$

Now, let $\omega(n)$ denote the number of computations for an n-point FFT. Then, after some manipluation of the matrix form of the above equation, the Gauss doubling formula with $n = 2^M$ yields

$$\begin{aligned}
\omega(n) &= 2\omega(n/2) + 2n \\
&= 2(2\omega(n/4) + 2(n/2)) + 2n \\
&= 4\omega(n/4) + 4n \\
&= 4(2\omega(n/8) + 2(n/4)) + 4n \\
&= 8\omega(n/8) + 6n \\
&\vdots \\
&= n\omega(1) + 2Mn \\
&= n + 2n\log_2 n \qquad \text{since } \omega(1) = 1 \\
&= O\left(n\log_2 n\right).
\end{aligned}$$

Hence the operation cost of the FFT is $O\left(n\log_2 n\right)$, which is a significant improvement to the operation cost $O(n^2)$ of the DFT.

4.2 Parameterizing the Boundary

Before we move on we should note, Theodorsen's method makes two demands of our data:

1. that the boundary be "star-like" with respect to an interior point (we will choose the origin). That is, that our boundary be of the form,

$$\gamma(\phi) = \rho(\phi)e^{i\phi}, \quad \rho(\phi) > 0, \quad \text{and } \phi \in [0, 2\pi]$$

2. that the boundary be sufficiently close to a circle for the method to converge.

For that reason, prior to applying Theodorsen's Method, we first:

1. smoothed the data by applying Karman-Trefftz (see section 3.3);

2. centered the image of the data and transformed it from Cartesian to polar coordinates.

It is at this point that we can now begin the process of forming the star-like parameterization of our data by interpolating by interpolating the radius $\rho(\phi)$.

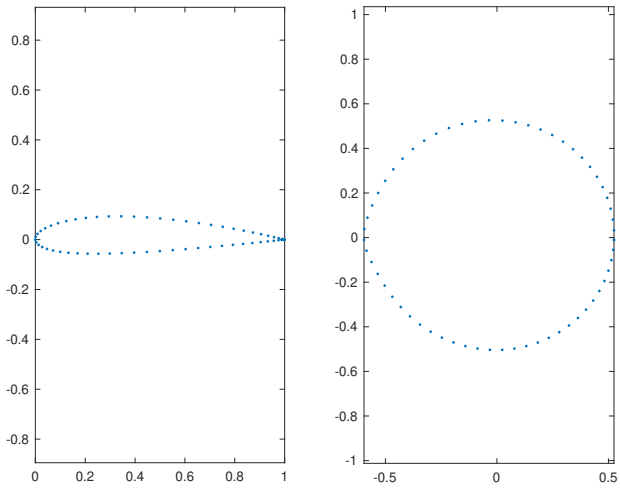

Figure 4.2.1: Discrete boundary points of a NACA 2415 airfoil and their image under the Karman-Trefftz map

After translating the points on the smooth curve to center them at the origin, the data for the spline fit is $\rho_i = \rho(\phi_i), i = 1, \ldots, n+1$. Interpolation by a periodic cubic spline with $\rho(\phi_1) = \rho(\phi_{n+1}) = \rho_1$ results in an $n \times n$ tridiagonal linear system with nonzero entries in

the $(1, n)$ and $n, 1)$ positions. This is solved efficiently by a method adapted from [13]. To do this we:

1. fitted periodic splines through the data;

2. formed $\rho(\phi)$ by interpolating the periodic splines.

4.2.1 Code

We will present the code for steps 2-4 here, for Karman-Trefftz see Sec 3.2.1:
Centering the data:

```
function [x1, y1, x, y] = centering(x,y)
    x1 = mean(x);
    y1 = mean(y);
    % Centers data onto the origin
    x = x - mean(x);
    y = y - mean(y);
end
```

Putting the Data in Polar Form:

```
function [theta, rho] = sendToPolar(x,y)
    % Takes (x,y) data and sends it to polar coordinates
    % Initialize arrays
    rho=[];
    theta=[];
    % Forms theta
    theta=atan2(y,x);
    % Converts from (-pi, pi) to (0, 2*pi)
    theta=mod(theta, 2*pi);
    theta(1)=0;
    theta(length(theta)+1)=theta(1)+2*pi;
    % Computes rho
    rho=sqrt(x.^2 + y.^2);
    rho(length(rho)+1)=rho(1);
end
```

Forming the Periodic Spline:

```
function [x1, x2, x3, h, tl] = perSpline(theta,rho)
    % Revised for star-like parametrization rho = rho(theta) for Theodorsen
    x = rho(:);
    if abs(x(1) - x(end)) > 100*eps
       x(end+1) = x(1);
    end
    n1 = length(x);
    n = n1 - 1;
    dx = diff(x);
    h = diff(theta);
    h = h(:);
    tl = sum(h);
    h(n1) = h(1);
    p = h(1:n);
    q = h(2:n1);
    a = q./(p + q);
    b = 1 - a;
    c = spdiags([[b(n);ones(n-1,1)] [a(2:n);0] [2*ones(n,1)] [0;b(1:n-1)] [
        ones(n-1,1);a(1)]] ...
                  , [-n+1 -1 0 1 n-1], n, n);
    d1 = 3*(a.*dx./p + b.*[dx(2:n); x(2) - x(n1)]./q);
    mmdflag = spparms('autommd');
    spparms('autommd', 0);
    x1 = c\d1;
    spparms('autommd', mmdflag);
    x1(2:n1) = x1;
    x1(1) = x1(n1);
    x2(2:n1) = 2*(x1(1:n) + 2*x1(2:n1) - 3*dx./p)./p;
    x2(1) = x2(n1);
    x2 = x2';
    x3  = diff(x2)./p;
    x3(n1) = x3(1);
```

Interpolating:

```
function fval = interp_perSpline(x, x1, x2, x3, h, tl, s)
    % Revised for a single periodic spline for starlike parametrization
    x = x(:);
    s = s(:);
    n1 = length(x);
    nn = n1 - 1;
    n = length(s);
    s = s - floor(s/tl)*tl;
    cumsumh = [0; cumsum(h(1:nn))];
    ppx = mkpp(cumsumh, [x3(1:nn)/6; x2(1:nn)/2; x1(1:nn); x(1:nn)]);
    fval = ppval(ppx,s);
```

4.3 Conjugate Periodic Functions

Given the conjugate periodic functions

$$\begin{cases} \phi(\theta) = u(1,\theta) \\ \psi(\theta) = v(1,\theta) - b_0, \end{cases}$$

the *conjugation operator* K is defined

$$\begin{cases} \phi(\theta) = a_0 + \sum_{n=1} a_n \cos(n\theta) + b_n \sin(n\theta) \\ -K\phi(\theta) := \psi(\theta) = \sum_{n=1} -a_n \sin(n\theta) + b_n \cos(n\theta) \end{cases}$$

So $v(1,\theta) - b_0 = -K\phi(\theta) = -F^{-1}\hat{K}Fu(1,\theta)$ and $K = F^{-1}\hat{K}F$, where F and F^{-1} are the Fourier and inverse Fourier transforms and

$$\hat{K} = \begin{cases} a_n \to -b_n \\ a_0 \to 0 \\ b_n \to a_n. \end{cases}$$

For $h(\theta) = \sum_{n=-\infty}^{\infty} c_n e^{in\theta}$, K still factors as $K = F^{-1}\hat{K}F$. But in this case

$$\hat{K} = \begin{cases} c_n \to -ic_n & n > 0 \\ c_0 \to 0 & \\ c_n \to ic_n & n < 0, \end{cases}$$

so that $-Kh(\theta) = -\sum_{n=-\infty}^{-1} ic_n e^{in\theta} + \sum_{n=1}^{\infty} ic_n e^{in\theta}$

4.3.1 Code

The Conjugation Operation:

```
function a = conjug(c)
    % Discrete conjugation using complex FFT
    n = length(c);
    n1 = (length(c))/2;
    k = 2:n1;
    a = fft(c);
    a(1) = 0;
    a(n1 + 1) = 0;
    a(k) = - i*a(k);
    a(n1 + k) =  i*a(n1 + k);
    a = ifft(a);
```

CHAPTER 5

Theodorsen's Method

5.1 Theodorsen's Method

Recall, that we require the boundary Γ be represented by the star-like parameterization $\gamma(\phi) = \rho(\phi)e^{i\phi}$ w.r.t. the origin, $\phi \in [0, 2\pi]$, and $0 < \rho(\phi)$. Theodorsen's method finds the boundary correspondence $\phi = \phi(\theta)$ for a conformal map $w = f(z)$ from the exterior of the unit disk to the exterior of Ω by successive conjugation. Using the normalization $f(\infty) = \infty$ and $0 < a_1 = f'(\infty) \in \mathbb{R}$.

Now, let's define $h(z)$, analytic for $|z| > 0$ to be the *auxiliary function*,

$$h(z) \coloneqq \log\left(\frac{f(z)}{z}\right).$$

Then

$$\mathrm{Im}\{h(e^{i\theta})\} - \mathrm{Im}\{h(\infty\} = -K\,\mathrm{Re}\{h(e^{i\theta})\}$$

and

$$h(\infty) = \log f'(\infty) = \log a_1.$$

But a_1 is real valued(see chapter 3), therefore $\mathrm{Im}\{h(\infty)\} = 0$.

And, since $f(e^{i\theta}) = \rho\left(\phi(\theta)\right)e^{i\phi(\theta)}$ we have that,

$$h(e^{i\theta}) = \log\left(\frac{\rho\left(\phi(\theta)\right)e^{i\phi(\theta)}}{e^{i\theta}}\right)$$

$$= \log\rho\left(\phi(\theta)\right) + i\left(\phi(\theta) - \theta\right)$$

Notice, this means $h(e^{i\theta})$ is of the form $u(1,\theta) + iv(1,\theta)$ where

$$\begin{cases} u(1,\theta) = \log\rho\left(\phi(\theta)\right) \\ v(1,\theta) = \phi(\theta) - \theta \end{cases}.$$

Now, we apply the conjugation operator K to the real and imaginary parts of $h(e^{i\theta})$. And, as $v(0,\theta) = 0 = b_0$, we get *Theodorsen's equation* for the exterior case,

$$\phi(\theta) - \theta = -K \log \rho\left(\phi(\theta)\right)$$

Fixing $\phi(0)$ with $0 \leq \phi(0) < 2\pi$ for uniqueness, we can solve this equation by application of Theodorsen's Iteration

$$\phi^{(0)}(\theta) - \theta = 0 \quad \text{(initial guess)}$$

$$\phi^{(n+1)}(\theta) - \theta = -K \log \rho\left(\phi^{(n)}(\theta)\right)$$

We will show that $\phi^{(n)}(\theta) \to \phi^{(exact)}(\theta), n \to \infty$ under suitable conditins on Γ. First we need the following estimate.

Lemma 5.1.1. $\|K\|_2 = 1$.

Proof. Recall $K : L^2[0,2\pi] \to L^2[0,2\pi]$. Let $u \in L^2[0,2\pi]$ and

$$\begin{aligned} u(\theta) &\sim a_0 + \sum_{n=1}^{\infty} a_n \cos n\theta + b_n \sin n\theta, \\ \|u\|_2^2 &= |a_0|^2 + \sum_{n=1}^{\infty} |a_n|^2 + |b_n|^2, \quad \text{and} \\ \|Ku\|_2^2 &= \sum_{n=1}^{\infty} |a_n|^2 + |b_n|^2. \end{aligned}$$

Therefore, $\|Ku\|_2 \leq \|u\|_2$ and if $a_0 = 0$, then $\|Ku\|_2 = \|u\|_2$. Therefore $\|K\|_2 = 1$. □

Note, $\|K\|_2$ is an *induced norm* for the operator K. Recall that such operator (or matrix) norms are defined from a given function space (or vector space) norm $\|\cdot\|$ as $\|K\| := \max_{\|h\|=1} \|Kh\|$ and the important property for making estimates and bounding quantities is that $\|Kh\| \leq \|K\|\|h\|$.

We now show that the Theordorsen iterations converge if the boundary satisfies the so-called $\epsilon -$ *condition*.

Theorem 5.1.2. *Let* $\epsilon := \sup_\phi |\frac{\rho'(\phi)}{\rho(\theta)}|$. *If* $\epsilon < 1$, *then* $\lim_{n\to\infty} \|\phi(\theta) - \phi^{(n)}(\theta)\|_2 = 0$.

Proof. From the Theodorsen iteration, we see that

$$\begin{aligned}
\|\phi(\theta) - \phi^{(n+1)}(\theta)\|_2 &= \|K[\log\rho(\phi(\theta)) - \log\rho(\phi^{(n)}(\theta))]\|_2 \\
&\leq \|\log\rho(\phi(\theta)) - \log\rho(\phi^{(n)}(\theta))\|_2 \\
&= \|\int_{\phi^{(n)}(\theta)}^{\phi(\theta)} \frac{\rho'(\theta)}{\rho(\theta)} d\theta\|_2 \\
&\leq \epsilon\|\phi(\theta) - \phi^{(n)}(\theta)\|_2.
\end{aligned}$$

Therefore, the iterations converge in the 2−norm, if $\epsilon < 1$. □

5.1.1 Code

Exterior Theodorsen's Method:

```
function f = theoext(n, f, itmax, rho, x1, x2, x3, h, tl)
    % Theodorsen s method for exterior regions
    % Initial guess for boundary correspondence
    th = 2*pi*[0:n-1]/ n;
    phi = th;
    phil = phi;
    disp('Iteration no.  Error between successive iterates');
    % Start of Theodorsen loop
    for it = 1 : itmax
        c = log(abs(f));
        % Conjugation
        c = -conjug(c);
        % Compute new boundary corespondence and calcuate errors
        phi = real(c) + th;
        error=max(abs(phi-phil));
        phil=phi;
        fprintf('%6.0f%30.14e\n', it, error);
        rhoeval = interp_perSpline(rho,x1,x2,x3,h,tl,phi);
        f = rhoeval'.*exp(1i*phi);
    end
```

5.2 Normalization of Theodorsen's Method

The normalization for the Theodorsen map $\zeta = f(z)$ from the exterior of the disk to the exterior of the closed curve, $\gamma(\phi) = \rho(\phi)e^{i\phi}$, is

$$f(z) = a_1 z + \sum_{j=0}^{\infty} \frac{a_{-j}}{z^j},$$

where $a_1 > 0$. That is f has a simple pole $f(\infty) = \infty$ at $z = \infty$ and $f'(\infty) > 0$. In order to apply the Kutta condition, we need to rotate the unit circle so that $f(1)$ maps to the

image of the trailing edge on the smooth curve $f(1) = \zeta_1 - c = \rho(1)$, where c is the center of the smooth curve, since our starlike parametrization of the boundary has $\rho(0) = \rho_1$. We, therefore, need to find the angle θ_{tr}, where

$$f(e^{i\theta_{tr}}) = \rho_1.$$

We have tried this using two methods: Solving $f(e^{i\theta_{tr}}) = \rho_1$ for $e^{i\theta_{tr}}$ by Newton's method or by interpolating the inverse $\theta = \theta(\phi)$ of the boundary correspondence at the Fourier points, $(\theta_i = 2\pi(i-1)/N, \phi_i), i = 1, \ldots, N, (2\pi, \phi_N + 2\pi)$, computed by the Theordorsen iterations, with a cubic spline and setting $\theta_{tr} = \theta(0)$, if $\phi_1 < 0$, and $\theta_{tr} = \theta(2\pi)$, if $\phi_1 > 0$. Both methods give similar results. The accuracies are limited by the spline interpolation and the accuracy of the mapping; see Table 5.1.

Table 5.1: The values of the angle of the image of the trailing edge on the unit circle (*angtheo* in the code) computed by Theordorsen's method using the spline fit or Newton's method. Note that the number of correct digits increases by about 1 each time N is double indicating the roughly $O(N^{-3})$ accuracy expected by the spline fits. Note also that the angle depends only on the airfoil and not on the angle of attack.

N	spline	Newton
32	-0.018200117390517	-0.018182051778078
64	-0.018388548886676	-0.018425772325956
128	-0.018419768716229	-0.018416359631915
256	-0.018416494188328	-0.018416443147069
512	-0.018416413704615	-0.018416419384364

5.2.1 Code

Normalization of Theodorsen's Method - Newton's Method:

```
% Newton's method for tr such that f(tr) = rho(1)
tr = 1; % initial guess
for k=1:10
    p(1:n - 2) = c(3:n);
    p(n - 1) =c(1);
    p(n) = c(2);
    ftr =  tr*polyval(p, tr^(-1));
    fptr = c(2)*tr;
    coeff=[(n/2-1:-1:1),0,0].*[c(n/2+2:n) 0 0];
    fptr  = fptr - polyval(coeff,1/tr);
    tr = tr + (rho(1) - ftr)/fptr;
    abs(tr);
end
angtheo = angle(tr)
```

Normalization of Theodorsen's Method - Spline Method:

```
% Spline method for tr such that f(tr) = rho(1)
if phi(1) <= 0
        angtheo = spline(phi(1:n), 2*pi*(0:(n - 1))/n, 0);
        angtheo = spline([phi(1:n) phi(1)+2*pi], 2*pi*(0:n)/n, 0);
elseif phi(1)>0
        angtheo = spline(phi(1:n), 2*pi*(0:(n - 1))/n, 2*pi) - 2*pi;
        angtheo = spline([phi(1:n) phi(1)+2*pi], 2*pi*(0:n)/n, 2*pi) - 2*pi;
end
```

CHAPTER 6

Numerical Examples

6.1 Review

In this chapter, we will apply the material and MATLAB code covered in the previous chapters to compute potential flows over a single airfoil. The reader may refer to chapters 2 through 5 for all of the necessary background material in complex analysis, Fourier series, conformal mapping, and potential flow. Here is a brief outline of the how we will apply the previous material:

1. In section 6.2, we smooth discrete data representing the boundary of a NACA 2415 airfoil by applying Karman-Trefftz. Next, we center and interpolate a periodic spline through the image of our data under Karman-Trefftz. Finally, we apply Theodorsen's Method to map the exterior of the unit disk to the exterior of our interpolants.

2. In section 6.3, we calculate the circulation about our airfoil.

3. In section 6.4, we solve for the streamlines of a uniform flow, various angles of attack, about the unit disk. Then we apply the inverse maps to find the flow in the KT and physical domains.

4. Finally, in section 6.5, we calculate the pressure curve about the airfoil.

6.2 NACA 2415 Airfoil

We compared results from our calculations to data from [12]. Using 128 Fourier points and a maximum of 100 iterations, we found Theodorsen's method converged to within machine epsilon after 25 iterations on our data.

```
For n = 2 ^ m Fourier points, m = 7
Enter maximum number of iterations, itmax = 100
Iteration no.  Error between successive iterates
     1          9.03959053963086e-02
     2          1.88101169449113e-02
     3          2.85558454886958e-03
     4          6.86770436595818e-04
     5          1.67327439827059e-04
     6          4.27456081064648e-05
     7          1.09123161293745e-05
     8          2.71404209550852e-06
     9          7.42707724654679e-07
    10          1.75019060577597e-07
    11          5.16105633785457e-08
    12          1.14784564075876e-08
    13          3.63532715041970e-09
    14          7.65816743353298e-10
    15          2.58713939160771e-10
    16          5.74198466551934e-11
    17          1.85642612393622e-11
    18          4.32054392263126e-12
    19          1.34070532453734e-12
    20          3.23741033980696e-13
    21          9.76996261670138e-14
    22          2.44249065417534e-14
    23          7.10542735760100e-15
    24          1.77635683940025e-15
    25          8.88178419700125e-16
    26          8.88178419700125e-16
    27          8.88178419700125e-16
    28          8.88178419700125e-16
```

Figure 6.2.1: The error between successive iterates for the first 28 out of 100 iterations.

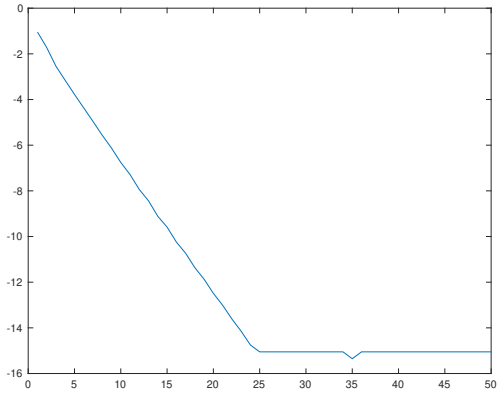

Figure 6.2.2: Theodorsen's method converged to within machine epsilon in 25 iterations on our data.

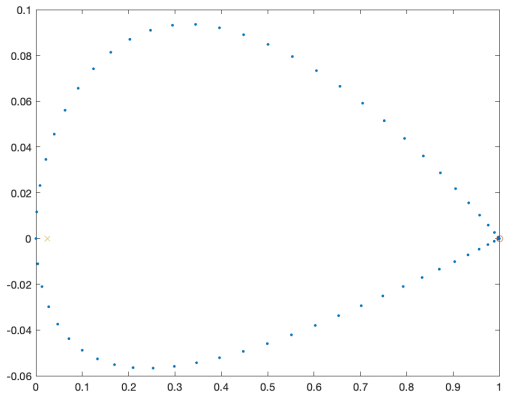

Figure 6.2.3: "x" is the interior point by Karman-Trefftz and "o" is the *sharp* boundary point.

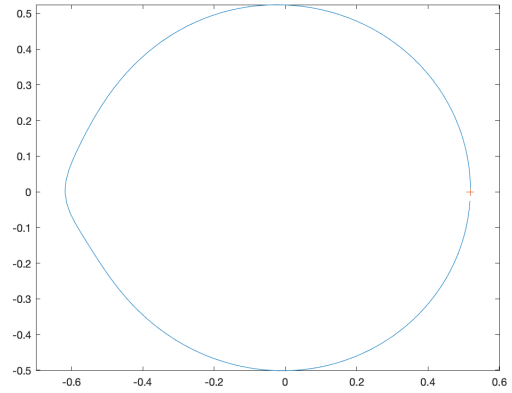

Figure 6.2.4: "+" is the image of the trailing edge.

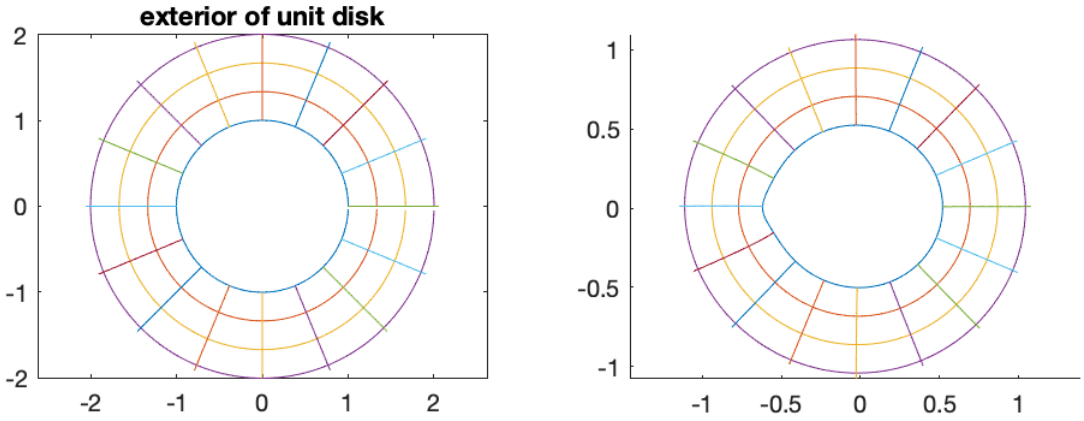

Figure 6.2.5: Orthogonal grid image of the exterior of the unit disk and the exterior of its image of the under Theodorsen's Method.

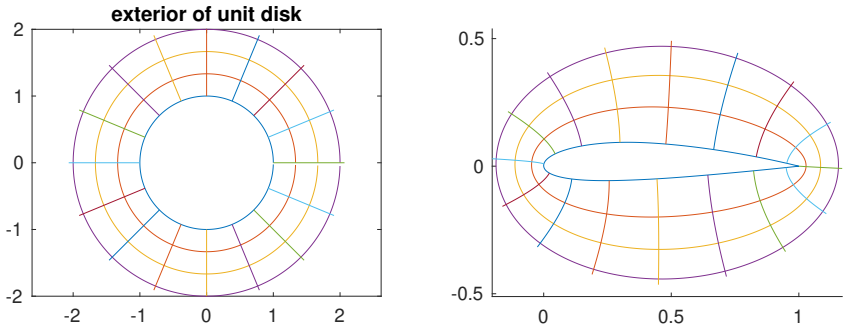

Figure 6.2.6: Orthogonal grid image of the exterior of the unit disk and its image under the composition of Karman-Trefftz and Theodorsen's to the exterior of the original airfoil.

6.3 Calculation of Circulations about NACA 2415

Here are some calculations of circulations for various angles of attack α and Fourier points N, Table 6.1. Again, the roughly $O(N^{-3})$ accuracy coming from the spline through the derivative $f'(\infty)$ is seen. The spline approximation is used here for the normalization $f(1) =$ trailing edge. The results agree well with calculations using Fornbergs method [9] in place of Theodorsen's method.

Table 6.1: Circulations $-\frac{\Gamma}{2\pi} = 2\text{Im}\{f'(\infty)Ue^{-i\alpha}\}$ with $U = 1$.

N	$f'(\infty)$	$\alpha = 0^o$	$\alpha = 5^o$	$\alpha = 10^o$
32	0.281445194681256 - 0.010696660343550i	0.021393320687101	0.070371042613474	0.118813198414362
64	0.281442326882906 - 0.010749508267709i	0.021499016535417	0.070475836366987	0.118916292529331
128	0.281441852891772 - 0.010758680244336i	0.021517360488672	0.070494027893863	0.118934193181323
256	0.281441887400038 - 0.010757722206302i	0.021515444412604	0.070492125124230	0.118932318199351
512	0.281441888476559 - 0.010757695887751i	0.021515391775502	0.070492072875078	0.118932266735797

6.4 Potential Flow about NACA 2415 using Theodorsen's Method

Using `ode45` we numerically solve the system

$$\begin{cases} \frac{dx}{dt} = \text{Re}\{w'(z)\} \\ \frac{dy}{dt} = -\text{Im}\{w'(z)\} \end{cases}$$

and plot the resulting streamlines.

The following are graphs of the potential flow, assuming various angles of attack, about the NACA 2415 airfoil (left), the image of the airfoil under Karman-Trefftz (center), and the unit circle. In each graph the "$\circ$" in the image on the left marks the point just to the interior of the leading edge of the airfoil, while the "x" marks the trailing edge. Similarly, in the center image the point just to the interior of the leading edge is marked with a "$\circ$" and the trailing edge with "$\otimes$" denoting the tailing edge. Finally, in the image on the right, "$\otimes$" marks the trailing edge on the unit circle.

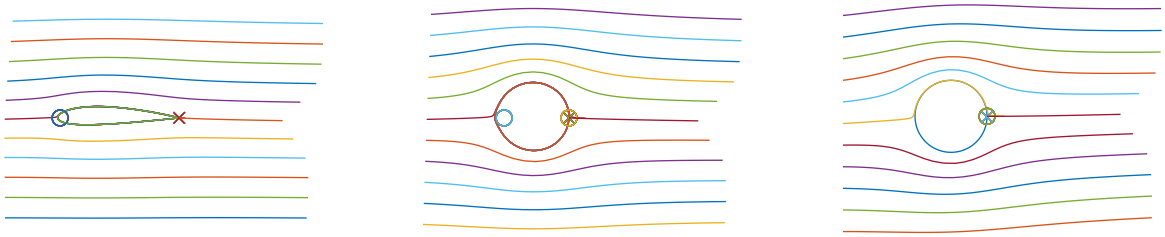

Figure 6.4.7: Assuming a 0° angle of attack.

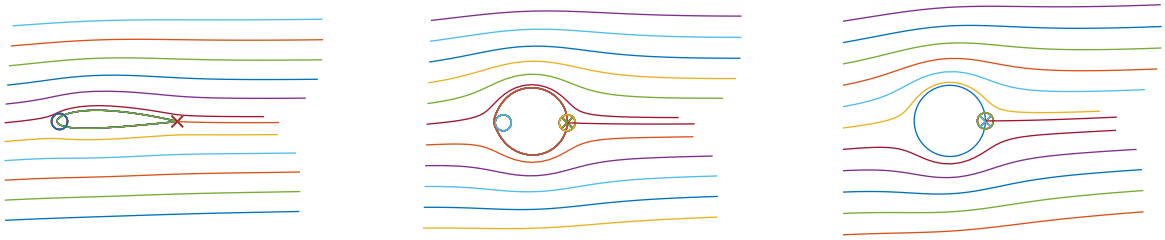

Figure 6.4.8: Assuming a 2° angle of attack.

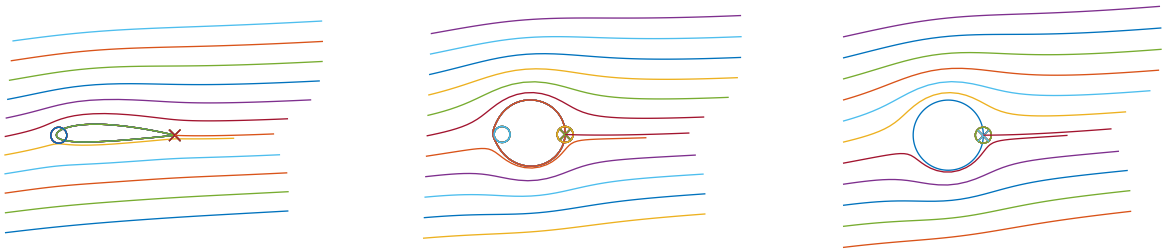

Figure 6.4.9: Assuming a 5° angle of attack.

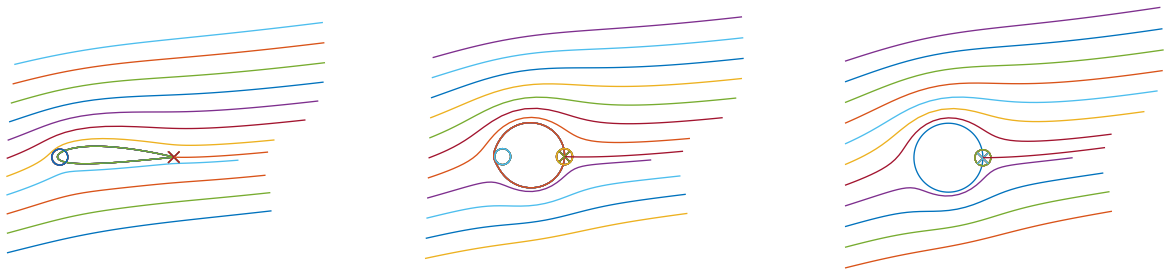

Figure 6.4.10: Assuming a 10° angle of attack.

6.5 Pressure about NACA 2415 using Theodorsen's Method

Using the results from our previous two sections, we calculate $\frac{dw}{dz}$ at the boundary about the circle to find the pressure about the the boundary of the NACA 2415 airfoil.

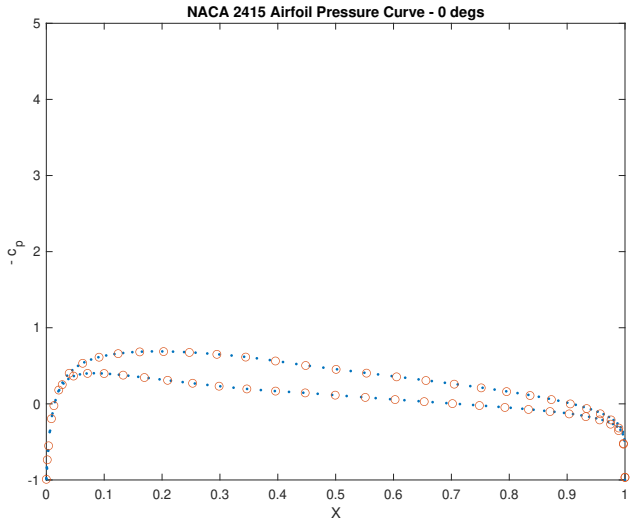

Figure 6.5.11: Graph of the predicted (·) pressure about the airfoil vs the measured (∘) pressure about the airfoil given a 0° angle of attack.

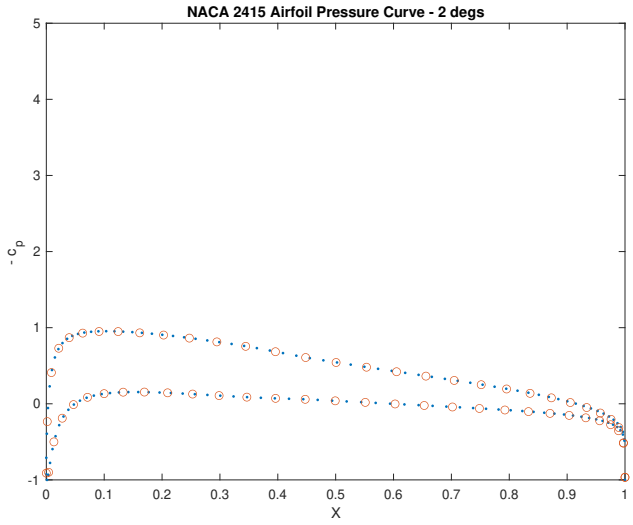

Figure 6.5.12: Graph of the predicted (·) pressure about the airfoil vs the pressure data from [12] (○) about the airfoil given a 2° angle of attack.

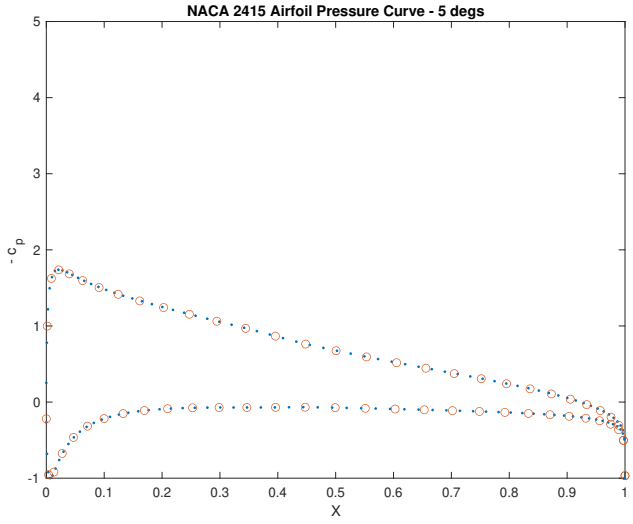

Figure 6.5.13: Graph of the predicted (·) pressure about the airfoil vs the pressure data from [12] (○) about the airfoil given a 5° angle of attack.

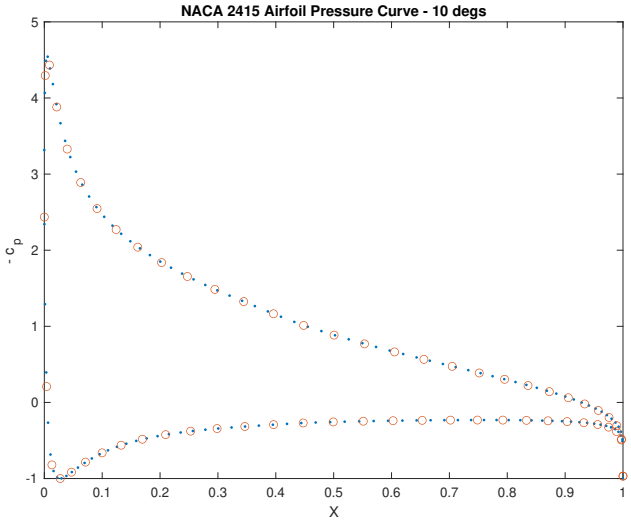

Figure 6.5.14: Graph of the predicted ($\cdot$) pressure about the airfoil vs the pressure data from [12] ($\circ$) about the airfoil given a 10° angle of attack.

CHAPTER 7

Conclusions and Future Work

A MATLAB code has been developed using Theodorsen's method to compute potential flow over single airfoils. The normalization of the Theodorsen map was adjusted so that the Kutta condition could be applied at the trailing edge of the airfoil. The code was tested for a NACA 2415 airfoil and the results compared well with calculation using a standard engineering code [12].

In future work, Theodorsen's method will be compared to other numerical conformal mapping methods for simply connected domains, such as the methods of Fornberg, Wegmann, Timman/James, and Prosnak, discussed in [6, 9, 11]. Other quantities of engineering interest, such as lift coefficients and moments, will be computed and additional airfoils will be tested; see [1]. This work will provide background for ongoing work on multi-element airfoil configurations [7, 8].

REFERENCES

LIST OF REFERENCES

[1] I. H. Abbott and A. E. von Doenhoff, *Theory of Wing Sections, including a summary of airfoil data*, Dover, 1959.

[2] D. J. Acheson, *Elementary Fluid Dynamics*, Oxford, 2005.

[3] L. Ahlfors, *Complex Analysis- An Introduction to the Theory of Analytic Functions of One Complex Variable*, McGraw-Hill, 2nd ed., 1966.

[4] S. Childress, *An Introduction to Theoretical Fluid Mechanics*, Courant Lecture Notes 19, AMS, 2009.

[5] T. K. DeLillo, *Numerical Conformal Mapping with Fourier Series Methods*, manuscript, in preparation.

[6] T. K. DeLillo and A. R. Elcrat, *A comparison of some numerical conformal mapping methods for exterior regions*, SIAM J. Sci. Comput., 12, 2 (1991), pp. 399–422.

[7] T. K. DeLillo and C. C. Green, *Computation of plane potential flow past multi-element airfoils using the Schottky-Klein prime function*, to appear in to Physica D.

[8] T. DeLillo, J. Mears, and S. Sahraei, *Computation of potential flow in multiply connected domains using conformal mapping*, submitted for publication.

[9] T. K. DeLillo and J. A. Pfaltzgraff, *Numerical conformal mapping methods for simply and doubly connected regions,* SIAM Journal on Scientific Computing Special Issue on Iterative Methods, 19 (1998), pp. 155–171.

[10] N. D. Halsey, *Potential flow analysis of multielement airfoils using conformal mapping*, AIAA J., 17 (1979) 1281-1288.

[11] P. Henrici, *Applied and Computational Complex Analysis*, Vol. III. Wiley, New York (1986).

[12] M. Hepperle, *Javafoil*, https://www.mh-aerotools.de/airfoils/javafoil. htm, [retrieved 8 August 2019].

[13] W. D. Hoskins and P. R. King, *Periodic cubic spline interpolation using parametric splines*, The Computer Journal, 15 (1972) 282–283.

[14] T. Theodorsen, *Theory of wing sections of arbitrary shape*, NACA Tech. Report 411, 1931.

LIST OF REFERENCES (continued)

[15] R. Wegmann, *Methods for numerical conformal mapping*, in *Handbook of Complex Analysis, Geometric Function Theory*, Vol. 2, (ed. R. Kuehnau), Elsevier, Amsterdam, (2005), 351–477.